Effect of thermo-mechanical process on structure and high temperature shape memory properties of Ti–15Ta–15Zr alloy*

Xiao-Hang Zheng(郑晓航)[1], Jie-He Sui(隋解和)[1], Zhe-Yi Yang(杨哲一)[1], Guo-Zhang Zhi(张治国)[2], and Wei Cai(蔡伟)[1,†]

[1] School of Materials Science and Engineering, Harbin Institute of Technology, Harbin 150001, China
[2] School of Science, Harbin Institute of Technology, Harbin 150001, China

(Received 26 September 2016; revised manuscript received 18 January 2017; published online 30 March 2017)

The effect of thermo-mechanical treatment on microstructure evolution, martensite transformation, and shape memory behavior of Ti–15Ta–15Zr high temperature shape memory alloy were investigated. Different martensite morphologies were found with different annealing temperatures. The Ti–15Ta–15Zr alloy exhibits almost perfect shape memory recovery strain of 6% after annealing at 973 K for 0.5 h.

Keywords: Ti–Ta–Zr alloy, thermo-mechanical treatment, high temperature shape memory effect

PACS: 61.66.Dk, 62.20.fg **DOI:** 10.1088/1674-1056/26/5/056103

1. Introduction

In recent years, high temperature shape memory alloys have attracted a great deal of attention due to their potential application in high temperature circumstances such as power generation and heating systems.[1–4] The high temperature shape memory alloys, including TiNi–X(Pd,Pt,Hf,Zr), NiMnGa, and β-Ti, Cu–Al–Ni, Zr–Cu based alloys, have been investigated.[2,3,5–8] They all have their advantages, for example, TiNiHf alloys have good shape memory effect, Ni–Mn–Ga alloys show good thermal stability, and Cu–Al–Ni and Zr–Cu alloys are economical for application. However, these alloys still have a number of problems which limit their practical application, for example, Ni–Ti–Pd/Pt has an ultrahigh cost due to the use of Pd/Pt, whereas Cu–Al–Ni, Ti–Ni–Hf, and Ni–Mn–Ga alloys are not sufficiently workable. Among these alloys, Ti-based alloys, including Ti–Nb, Ti–Mo, and Ti–Ta alloys, show excellent cold workability (thickness reduction is up to 90% by cold rolling), which makes them easy to be fabricated into various shapes for actual application.[7–10] However, for the above mentioned alloys, ω phase precipitation is easily formed during thermal cycles, leading to the brittleness, instability of martensitic transformation temperature and shape memory effect. The quantity of ω phase precipitation in Ti–Ta alloys is less than that in the other Ti-based alloys during thermal cycles with similar transformation temperature.[2,11] Hence, Ti–Ta alloy is thought to be a potential candidate for HTSMEs application. Our previous results show that with the addition of 10 at.% Zr as a substitute of Ta into Ti–Ta alloy, the martensite reverse transformation peak temperature A_p increases from 483 K to 750 K and the maximum shape memory recovery strain increases from 2.5% to 4.6% with 8% deformation.[12] The above results indicate that the addition of a ternary element, especially Zr, into Ti–Ta alloy is an effective way to increase the shape memory properties. Besides the addition of a ternary element, thermo-mechanical treatment is another effective method to improve the shape memory effects by grain refinement and a high density of thermally rearranged dislocations.[5,13–16] Therefore, the improvement on the shape memory effects of Ti–15Ta–15Zr alloy by thermo-mechanical treatment is expected. It is necessary to investigate the structure evolution with different annealing temperatures.

The effects of annealing temperature on structure, martensite transformation, and shape memory characteristics are investigated in this paper. The results show that the perfect shape memory recovery strain of 6% can be obtained at the proper annealing condition after cold working.

2. Experiment

The Ti–15Ta–15Zr alloy was prepared on a non-consumable arc-melting furnace under an Ar atmosphere using a water-cooled copper crucible from elemental constituents with purity of 99.9%. The arc-melting was repeated eight times to ensure the uniformity of composition. After melting, the ingots were homogenized at 1173 K for 6 h in vacuum-sealed quartz tubes, and then quenched in ice water. Cold rolling was performed up to 70% in thickness reduction. The thickness reduction for every rolling was limited to 2%–5%. The final thickness of the specimen after cold rolling was about 2 mm. The specimens were sealed in a vacuum quartz tube and annealed at different temperatures (673 K, 773 K, 873 K, 973 K, and 1073 K) for 0.5 h. The cold-rolled specimens were cut into desired shapes for various characteriza-

*Project support by the National Natural Science Foundation of China (Grant No. 51501049), China Postdoctoral Science Foundation (Grant No. 2015M571405), and the Fundamental Research Funds for the Central Universities, China (Grant No. HIT.NSRIF.20163).

†Corresponding author. E-mail: weicai@hit.edu.cn

© 2017 Chinese Physical Society and IOP Publishing Ltd

tions by a spark-erosion cutting machine.

The phase structure was identified by x-ray diffraction (XRD) on a Riguku-D/max-cB x-ray diffractometer with Cu $K\alpha$ radiation at room temperature. The microstructure was observed by transmission electron microscope (TEM, FEI TECNAI G2 20 STWIN 200 kV). The samples for TEM characterization were prepared by mechanically polishing to 70 μm and then twin-jet electro polishing in an electrolyte solution composite of 2 vol.% HF, 5 vol.% H_2SO_4, and 93 vol.% MeOH. The phase transformation temperature of the specimens was determined by differential scanning calorimetry (DSC, Perkin Elmer Diamond). The tensile stress–strain tests were performed on the Instron-5569 machine with a strain rate of 10^{-2} min^{-1}. The dimension length and the cross section of the tensile samples were 40 mm and 3 mm×1 mm, respectively.

3. Results and discussion

Figure 1 shows XRD profiles taken from the cold-rolled direction of the Ti–15Ta–15Zr alloy after cold working and annealing at different temperatures. The identical phase is α'' martensite with an orthorhombic structure without any impurity phase, which means that the M_s temperature is above room temperature and Zr atoms are dissolved into the martensite lattice. The XRD profile of the cold-rolled specimen shows the broad peaks of $(002)_{\alpha''}$, $(022)_{\alpha''}$, and $(113)_{\alpha''}$, indicating the presence of a deformed martensite. The peaks become sharper with the increase of the annealing temperature due to annihilation of internal stress and crystallization process. The relative intensity of the $(002)_{\alpha''}$ and $(111)_{\alpha''}$ peaks dramatically changes between the cold-rolled specimen and the specimen annealed at 973 K. With the increase of the annealing temperature, the positions of the peaks shift slightly to the left side, indicating the increase of the interplanar distance and the release of the internal stress. However, the $(002)_{\alpha''}$ and $(111)_{\alpha''}$ peaks are mixed together in the plane parallel to the cold-rolled direction. The cold-rolled plane is under tensile stress while the plane perpendicular to the cold-rolled direction is under compress stress during cold rolling. The intensities of the peaks from the two directions are different because of the severe deformation. In order to distinguish the $(002)_{\alpha''}$ and $(111)_{\alpha''}$ peaks, the XRD patterns taken from the direction perpendicular to the cold-rolling direction are shown in Fig. 2. The XRD profile of the solution-treated sample is also provided here for comparison. The patterns in the range from 35° to 45° are deconvoluted as shown in Fig. 2(b). The intensity ratio of the $(111)_{\alpha''}$ and $(002)_{\alpha''}$ peaks has been calculated. The $I_{(111)}/I_{(002)}$ of the cold-rolled specimen is about 2, while that of the specimen annealed at 973 K for 0.5 h is about 0.38. With further increasing the annealing temperature to 1073 K, the ratio is decreased to 0.23. The specimen annealed at 1073 K has the similar $I_{(111)}/I_{(002)}$ with the solution-treated one, indicating that the recrystallization is almost completed when annealed at 1073 K.

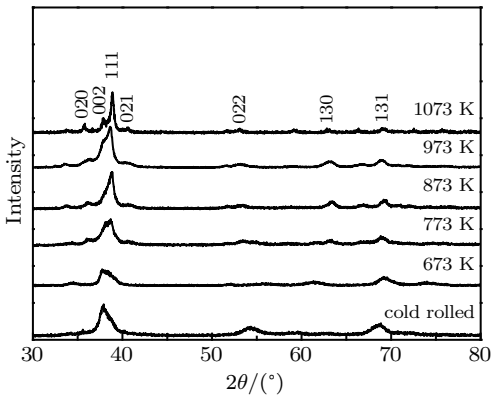


Fig. 1. XRD patterns taken from cold rolling direction of Ti–15Ta–15Zr alloy after cold deformation and annealing at different temperatures.

The TEM image of the cold-rolled Ti–15Ta–15Zr alloy is shown in Fig. 3(a). It can be seen that there are thick deformation bands with a lot of irregular dark areas caused by the stress contrast in the cold-rolled specimen. Also shown are some thin martensite variants in the thick martensite plate. Some of the martensite boundaries are either twisted or unclear because of the severe deformation. The annealing after cold rolling partially recovers the structure through rearrangement and annihilation of dislocations. Since the martensite reverse transformation start temperature A_s is higher than 673 K, after annealing at 673 K for 0.5 h, recovery only happens in the cold-rolled specimen, and the alloy retains the deformed martensite structure (Fig. 3(b)). In Fig. 3(c), the microstructure of the specimen annealed at 773 K does not show any obvious difference compared with that of the specimen annealed at 673 K, indicating that the recrystallization process has not taken place yet. With releasing of the internal stress, the internal annealing twin is observed in thick martensite plates. The substructure of martensite is indexed to type I twinning on $(111)_{\alpha''}$ where the beam direction is $[11]_{\alpha''}$. When the specimen is annealed at 873 K, which is above the martensite reverse transformation finish temperature A_f, the cold-rolled martensite transforms into the parent phase during annealing and transforms back into martensite on cooling. Thus, the morphology of martensite changes remarkably to the V-shape self-accommodation martenstie variants as shown in Fig. 3(c). However, the boundaries of the deformation band are preserved after annealing at 873 K. It is probably because at the primary recrystallization state, the release of the stored energy during cold-rolling is not sufficient for the transformation of the boundaries, so the boundaries disappear when the annealing temperature is increased to 973 K as shown in Fig. 3(e). It has been reported that due to the smaller grain size and the necessity to accommodate the mismatch across the grain boundaries, the martensitic transformation is expected to be more propagation controlled,[17] which will lead to a larger fraction of self-accommodated martensite variants, and a finer variant

structure as seen in Fig. 3(e). This microstructure will benefit the shape memory effect. Figure 3(f) shows the TEM image of Ti–15Ta–15Zr alloy annealed at 1073 K. Typical self-accommodation α'' martensite structures are clearly observed, indicating that the internal stress induced by cold rolling is fully released and the recrystallization is completed.

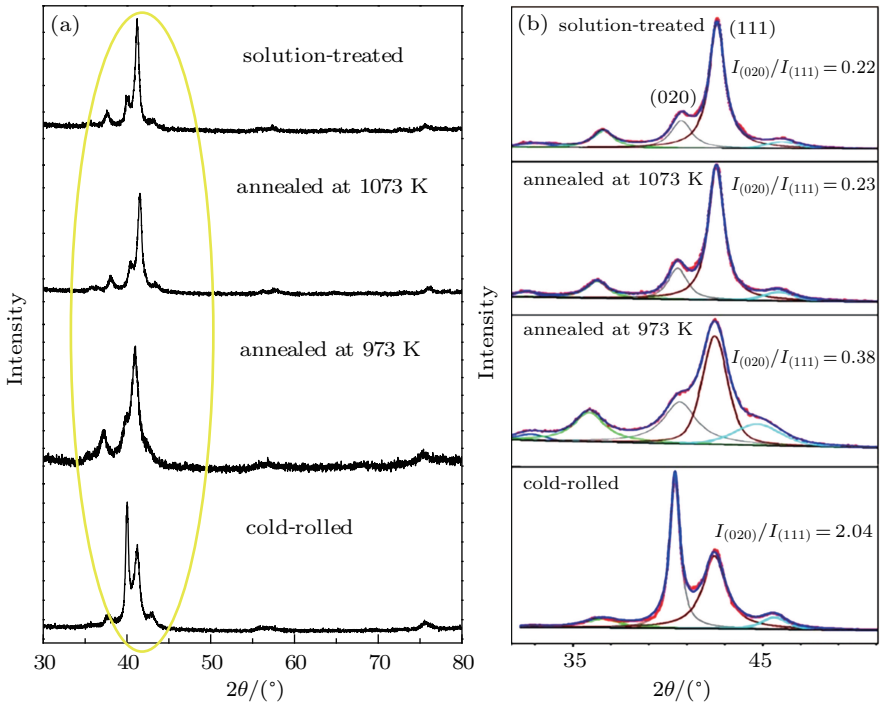


Fig. 2. (color online) XRD patterns taken from the direction perpendicular to the cold-rolling direction.

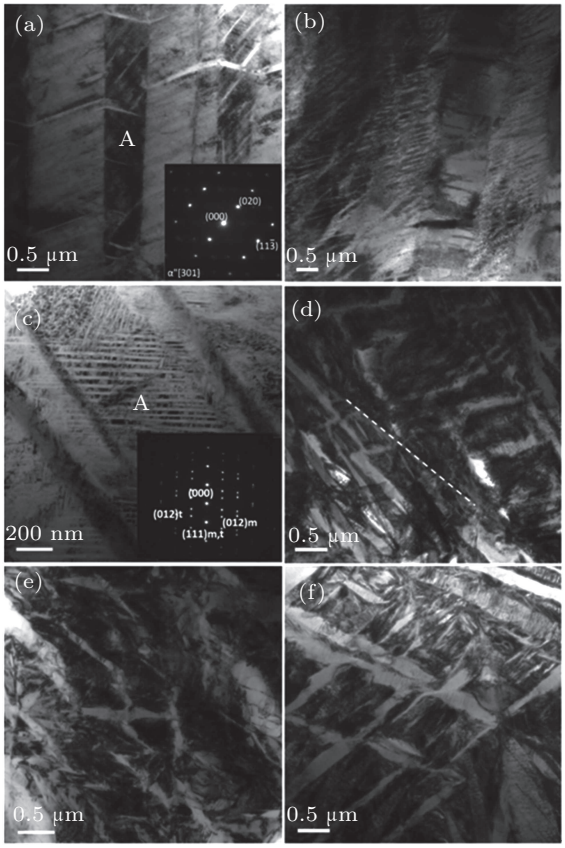


Fig. 3. TEM images of Ti–15Ta–15Zr alloy after (a) cold rolling and annealing at different temperatures: (b) 673 K, (c) 773 K, (d) 873 K, (e) 973 K, (f) 1073 K.

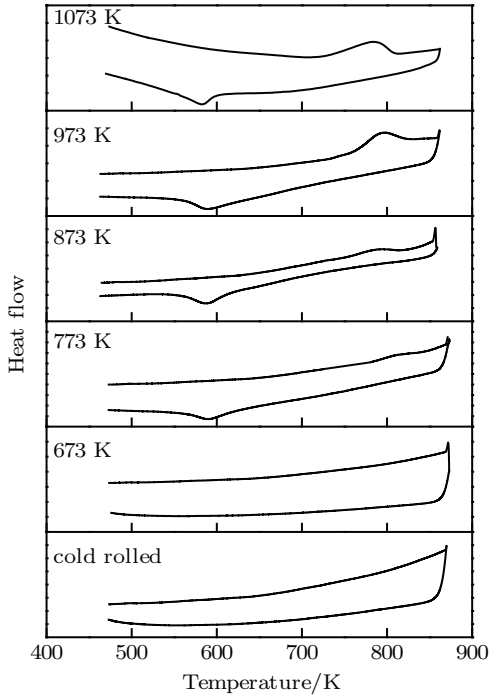


Fig. 4. DSC curves after cold deformation and annealing at different temperatures.

Figure 4 shows DSC curves of Ti–15Ta–15Zr with different annealing temperatures. Neither the cold-rolled specimen nor the specimen annealed at 673 K shows a martensite transformation peak. This suppression of martensite transformation

is due to the internal stresses induced by cold deformation. The small and broad martensite transformation peaks are observed in the curve of the specimen annealed at 773 K. The peaks become sharper and the transformation temperatures increase slightly with the increasing annealing temperature due to the recovery and recrystallization processes.

Figure 5 shows the stress–strain curves of Ti–15Ta–15Zr alloy with different annealing temperatures. According to the XRD results, the specimens annealed at different temperatures are in the martensite phase at room temperature. It can be observed that the specimen annealed at 673 K is broken without any yielding because of the high internal stress stored in the sample on cold rolling. There is only one yield stage in the specimen annealed at 773 K, which means that the plastic deformation and martensite variants reorientation occur at the same time. It can also be observed that the specimens annealed at higher than 873 K exhibit two-stage yielding, and the two stages correspond to the martensite variants reorientation and the plastic deformation, respectively. The failure strain increases and the ultimate tensile strength decreases with increasing annealing temperature due to annihilation of internal stress and recrystallization. The specimens annealed at lower temperature exhibit higher yield stress because of grain refinement.

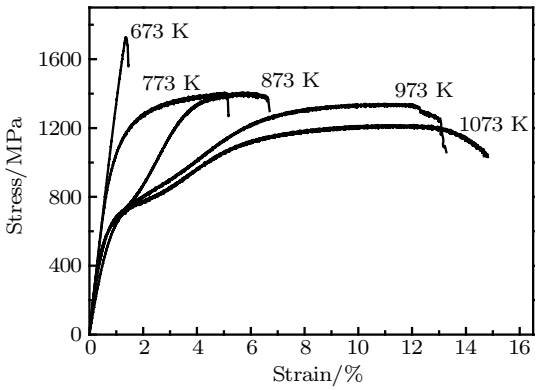


Fig. 5. Tensile stress–strain curves of Ti–15Ta–15Zr alloy annealed at different temperatures.

The specimens annealed at 973 K and 1073 K possess relative good ductility. Figures 6(a) and 6(b) show the stress–strain curves upon loading-unloading with different deformations after being annealed at 973 K and 1073 K, respectively. It can be seen that the specimen annealed at 973 K can obtain almost 6% full recovery strain, which is 2% higher than that of the specimen annealed at 1073 K. The maximum total recovery strain of 6.7% is obtained by the deformation of 8%.

The structures of the cold-rolled specimen and those annealing at different temperatures are proved to be orthorhombic structure martensite by the TEM and XRD results. The martensite is shown as a thick deformation band in the cold-rolled specimen, there is only very limited restoration occurring after annealing at 673 K for 0.5 h according to the TEM and XRD results. The high internal stress maintained in the specimen makes it brittle and impossible to have shape memory behavior. The crystal structure of the alloy is fully transformed to the parent phase when annealed at above A_f. With further increasing the annealing temperature to above A_f, the V-shape martensite and thermal rearrangement dislocations appear. On one hand, dislocations can enhance the critical share stress that is proportional to the square root of the dislocation density, which is beneficial to the shape memory effect. On the other hand, dislocations may block the reorientation of the martensite variants, resulting in the decrease of the shape memory effect. Therefore, a suitable amount of dislocation can increase the critical slip stress and improve the shape memory effect. When the specimen is annealed at 1073 K, a well-developed self-accommodation martensite is shown, indicating the recrystallization finish, which is consistent with the XRD results. The internal stress induced by cold-rolling is fully released and the grain size increases, leading to the decrease of the shape memory effects.

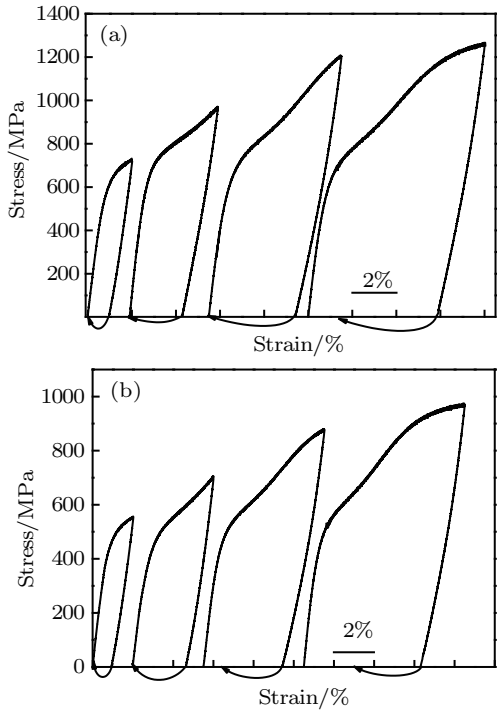


Fig. 6. Tensile stress–strain curves upon loading–unloading with different deformation after annealing at (a) 973 K and (b) 1073 K.

4. Conclusion

We investigated the effect of thermo-mechanical treatment on the structure and martensitic and shape memory properties of Ti–15Ta–15Zr alloy. Annealing at 973 K effectively increases the critical stress for plastic deformation and the shape memory behavior. The alloy annealed at 973 K shows almost perfect shape memory recovery strain of 6%.

References

[1] Ma J, Karaman I and Noebe RD 2010 *Inter. Mater. Rev.* **55** 257
[2] Meng F B, Guo H J, Liu G D, Liu H Y, Dai X F, Luo H Z, Li Y X, Chen J L and Wu G H 2009 *Chin. Phys. B* **18** 3031
[3] Tan C L, Tian X H and Cai W 2010 *Chin. Phys. B* **19** 037101
[4] Tian X H, Tan C L and Cai W 2012 *Chin. Phys. B* **21** 57105
[5] Kim H Y, Jinguu T, Nam T H and Miyazaki S 2011 *Script Mater.* **65** 846
[6] Shen H H, Fu H, Guo Y J, Fu Y Q and Zu X T 2011 *Chin. Phys. B.* **20** 46102
[7] Kim H Y, Ikehara Y, Kim J I, Hosoda H and Miyazaki S 2006 *Acta Mater.* **54** 2419
[8] Al-Zain Y, Kim H Y, Hosoda H, Nam T H and Miyazaki S 2010 *Acta Mater.* **58** 4212
[9] Buenconsejo P J S, Kim H Y and Miyazaki S 2009 *Acta Mater.* **57** 2509
[10] Buenconsejo P J S, Kim H Y and Miyazaki S 2011 *Scripta Mater.* **64** 1114
[11] Kim H Y, Fukushima T, Buenconsejo P J S, Nam T H and Miyazaki S 2011 *Mater. Sci. Eng. A* **528** 7238
[12] Zheng X H, Sui J H, Zhang X, Yang Z Y, Tian X H and Cai W 2013 *Scripta Mater.* **68** 1008
[13] Kim H Y, Kim J I, Inamura T, Hosoda H and Miyazaki S 2006 *Mater. Sci. Eng. A* **438** 839
[14] Arijit Sinha B M and Chattopadhyay P P 2013 *Mater. Sci. Eng. A* **561 338** 43
[15] Lin H C and Wu S K 1994 *Acta Mater.* **42** 1623
[16] Kitamura K, Miyazaki S, Iwai H and Kohl M 1999 *Mater. Sci. Eng. A* **273** 758
[17] Kim Jae II, Park Y C and Myeon Ock J 2013 *J. Alloys Compd.* 557 S453 ICOMAT2011